

The Structure of Alfalfa Mosaic Virus Capsid Protein Assembled as a T=1 Icosahedral Particle at 4.0-Å Resolution†

ABHINAV KUMAR,^{1,2} VIJAY S. REDDY,² VIDADI YUSIBOV,^{3,‡} PAUL R. CHIPMAN,¹ YASUO HATA,^{1,§} IGNACIO FITA,^{1||} KEIICHI FUKUYAMA,^{1,#} MICHAEL G. ROSSMANN,¹ L. SUE LOESCH-FRIES,³ TIMOTHY S. BAKER,¹ AND JOHN E. JOHNSON^{2,*}

Department of Biological Sciences¹ and Department of Botany and Plant Pathology,³ Purdue University, West Lafayette, Indiana 47907, and Department of Molecular Biology, The Scripps Research Institute, La Jolla, California 92037²

Received 1 April 1997/Accepted 21 June 1997

K. Fukuyama, S. S. Abdel-Meguid, J. E. Johnson, and M. G. Rossmann (J. Mol. Biol. 167:873–984, 1983) reported the structure of alfalfa mosaic virus assembled from the capsid protein as a T=1 icosahedral empty particle at 4.5-Å resolution. The information contained in the structure included the particle size, protein shell thickness, presence of wide holes at the icosahedral fivefold axes, and a proposal that the capsid protein adopts a β-barrel structure. In the present work, the X-ray diffraction data of Fukuyama et al. as well as the data subsequently collected by I. Fita, Y. Hata, and M. G. Rossmann (unpublished) were reprocessed to 4.0-Å resolution, and the structure was solved by molecular replacement. The current structure allowed the tracing of the polypeptide chain of the capsid protein confirming the β-sandwich fold and provides information on intersubunit interactions in the particle. However, it was not possible to definitively assign the amino acid sequence to the side chain density at 4-Å resolution. The particle structure was also determined by cryoelectron microscopy and image reconstruction methods and found to be in excellent agreement with the X-ray model.

Alfalfa mosaic virus (AMV), a member of the *Bromoviridae* family of plant viruses (22), occurs predominantly as bacilli-form particles composed of one of the four genomic RNAs and a surrounding shell built from a single gene product of 220 residues. These particles have a constant diameter but variable lengths depending on the size of RNA packaged (15, 16). In the absence of nucleic acid, AMV capsid protein (CP) subunits can be assembled into T=1 icosahedral particles (9) which can be crystallized (13). Crystallization is facilitated by the removal of the highly basic N-terminal arm of the CP through a mild trypsin treatment that removes the first 26 residues (4, 13).

X-ray crystallographic studies of this T=1 particle were undertaken in the early 1980s when 4.5-Å diffraction data were obtained from crystals of the truncated particles (2, 13). The electron density map that was obtained with phases computed by the single isomorphous replacement method and subsequent averaging using 20-fold noncrystallographic symmetry revealed a spherical particle about 210 Å in diameter and with prominent holes (~38 Å in diameter) at the icosahedral fivefold axes (12). Data acquired at higher resolution (~4.0 Å) were subsequently collected by Fita et al. and used, in conjunction with the results of Fukuyama et al. (12), to build a partial model of the CP (11). However, it was not possible to definitively determine the backbone topology of the CP.

We have since tried to grow better-quality crystals to extend

the resolution of the diffraction data and solve the structure of the CP at atomic resolution. Despite extensive efforts to grow crystals with plant-purified material as well as with genetically expressed protein (33), we have not obtained crystals that diffract beyond 4.0 Å. Meanwhile, the analysis of the existing diffraction data was reinitiated with improved programs, which resulted in an electron density map that revealed a β-barrel in the subunit region. The old film data (11, 13) were reprocessed, scaled, and postrefined. The model constructed by Fita et al. was used to compute initial phases for the molecular replacement procedure, and an electron density map that permitted the determination of the main chain fold of the subunit was obtained.

The structure of the T=1 particle was also obtained at low resolution (~27 Å) by cryoelectron microscopy (cryoEM) and image reconstruction methods. The X-ray model fits the envelope of the density defined by the cryoEM reconstruction with remarkable fidelity.

MATERIALS AND METHODS

X-ray analysis. The native X-ray diffraction patterns obtained from the crystals of AMV (11, 13) were reprocessed, scaled, and merged together by using the Purdue University suite of programs (24, 25). The merged data were postrefined with lattice constants and mosaicity as variables. The rotation function was calculated with the program GLRF (30). An initial set of phases between 20- and 15-Å resolution was generated with the program X-PLOR (6) from the model built by Fita et al. (11). The phases were refined by real-space averaging of the electron density, using 20-fold noncrystallographic symmetry by the program RAVE (18). Phase refinement proceeded with 15 to 20 cycles of real-space averaging at a given resolution until the phases converged to within 5°. The initial mask used for the averaging process was derived from the model of Fita et al. with the program MAMA (18). After the phase convergence at a given resolution, the averaged electron density was Fourier transformed to a higher resolution (at the rate of one reciprocal unit per extension) to obtain a new set of phases for the next round of phase refinement. The mask was revised and improved on the basis of the averaged electron density after each set of five extension steps. The refined phases were combined with the observed structure factors to compute an electron density map that was interpretable. A polyalanine model was built into the electron density with the program O (17). Most of the programs used in the phase extension and refinement process belong to the CCP4 suite of programs (7).

* Corresponding author. Phone: (619) 784-9705. Fax: (619) 784-2980. E-mail: jackj@scripps.edu.

† Manuscript no. 10691MB from The Scripps Research Institute.

‡ Present address: Institute for Biochemistry and Advanced Molecular Medicine, Thomas Jefferson University, Philadelphia, PA 19107.

§ Present address: Institute for Chemical Research, Kyoto University, Uji, Kyoto 611, Japan.

|| Present address: Departamento de Ingeniería Química, ETSIIB, 08028 Barcelona, Spain.

Present address: Department of Biology, Faculty of Science, Osaka University, Osaka 560, Japan.

TABLE 1. Comparison of data processing and phase refinement statistics^a

Data	Highest resolution (Å)	Rejection criterion ^c	R_{merge} (%)	No. of independent reflections (%)	R factor after phase refinement (%)	CC after phase refinement (%)
From reference 12	4.5	$I < 2\sigma$	11.56	23,207 (55.1)	35.0	68.0
Reprocessed	4.0	$I < 4\sigma$	10.55	42,665 (71.3)	29.3 ^b	81.7 ^b

^a Comparison of the processing statistics between the previously reported diffraction data of Fukuyama et al. (12) and the reprocessed data collected by Fita et al. and Fukuyama et al. (11, 12). The R factor and the CC comparing the observed structure factors with those calculated from the respective averaged electron densities are also reported.

$$R_{\text{merge}} = \frac{\sum_h \sum_i |I(\mathbf{h}) - I_i(\mathbf{h})|}{\sum_h I_i(\mathbf{h})}$$

where $I_i(\mathbf{h})$ is the intensity of the i th observation of a reflection \mathbf{h} (indices hkl) with a mean intensity of $I(\mathbf{h})$.

$$\text{CC} = \frac{\sum_h (|F_{\text{obs}}(\mathbf{h})| - \langle |F_{\text{obs}}(\mathbf{h}) \rangle) (|F_{\text{calc}}(\mathbf{h})| - \langle |F_{\text{calc}}(\mathbf{h}) \rangle)}{\left[\sum_h (|F_{\text{obs}}(\mathbf{h})| - \langle |F_{\text{obs}}(\mathbf{h}) \rangle)^2 \sum_h (|F_{\text{calc}}(\mathbf{h})| - \langle |F_{\text{calc}}(\mathbf{h}) \rangle)^2 \right]^{1/2}}$$

$$R = \frac{\sum_h ||F_{\text{obs}}(\mathbf{h})| - k|F_{\text{calc}}(\mathbf{h})||}{\sum_h |F_{\text{obs}}(\mathbf{h})|}$$

where $F_{\text{obs}}(\mathbf{h})$ is the experimentally measured structure factor amplitude for the reflection \mathbf{h} , $F_{\text{calc}}(\mathbf{h})$ is the corresponding amplitude obtained by inverse Fourier transforming the averaged electron density, and k is a scale factor between $F_{\text{obs}}(\mathbf{h})$ and $F_{\text{calc}}(\mathbf{h})$. The operation $\langle \rangle$ denotes the mean of the argument over a given resolution shell.

^b Calculated at 4.5-Å resolution for comparison with the statistics reported by Fukuyama et al. (12).

^c I and σ refer to the measured intensity and its standard error.

CryoEM and image reconstruction. The AMV particles were grown and harvested from tobacco plants and purified by established protocols (31). The virus particles were disassembled by incubating in a high-salt solution (2 M MgCl₂) which precipitated the RNA, and the purified CP subunits were allowed to reassemble into empty icosahedral particles by extensive dialysis against pyrophosphate buffer (50 mM pH 7.0) (9, 10, 13). The assembled T=1 particles were imaged by the cryoEM technique on a Philips EM420 transmission electron microscope under low-dose ($\approx 1,800\text{-e}^-/\text{nm}^2$) conditions at a nominal magnification of $\times 49,000$ and a defocus value of $\approx 1.2\ \mu\text{m}$. A micrograph that displayed uniform ice thickness with minimal drift and astigmatism, as determined by eye, was subjected to digitization (25- μm step size) and image analysis procedures as described previously (23). Of the 95 particles that were boxed from the selected micrograph, the orientations and origins of 21 particles were refined, and the images were used to calculate a three-dimensional reconstruction at 22-Å-resolution cutoff. An estimate of the actual resolution was determined by selecting two independent group of 20 particles each from the original 95-particle data set and comparing the reconstructions computed from each set. A reliability index, R_{AB} factor (3, 32), which compares structure factors for the two reconstructions, indicated that the resolution of the data was limited to $\sim 27\ \text{Å}$.

RESULTS AND DISCUSSION

X-ray analysis. The films were reprocessed to benefit from considerable improvements that have been made in the processing programs since they were originally used for the AIMV data processing in 1983 (12). Additionally, a better procedural strategy was adopted for processing. For instance, the processing program now allows the reflection centers to fall on non-integral raster points and does not shift them to the nearest integral points as originally performed with the older version of the program. The profile fitting to the reflection peaks was extended to four cycles on each film as rather than the two cycles used earlier. Owing to these and other improvements in the programs and processing strategy, the reprocessing of films and postrefinement of the merged data were considered essential in order to obtain a more accurate data set. A 71% complete data set to 4.0-Å resolution was obtained after the postrefinement. Table 1 documents the improvement in the quality of the reprocessed data compared to the previously reported data (12).

Rotation function analysis of the new data set was in agreement with that obtained by Abdel-Meguid et al. (2). The two virus particles are situated in the P6₃ hexagonal cell with their threefold icosahedral axes coincident with the crystal threefold axes and are related to each other by the crystal twofold screw axis. This unique orientation of the particles fixes their positions unambiguously in the a-b plane of the unit cell. In the polar P6₃ space group, the position along the c axis is arbitrary, and so the particle positions of (1/3, 2/3, 0) and (2/3, 1/3, 1/2) were chosen.

The statistics of phase refinement in various resolution shells at the convergence of refinement cycles at 4.0-Å resolution are listed in Table 2. The model building into the electron density was initiated at $\sim 5.5\text{-Å}$ resolution because at this resolution features of the protein, such as a helix and a beta strand, became discernible. The quality of the map at 5.0-Å resolution was sufficiently good to position a canonical β -barrel into the density, with the initial alignment of the wall comprised of strands βB , βI , βD , and βG . Only at higher resolution ($\sim 4.5\ \text{Å}$) did strands βC , βH , βE , and βF of the other wall of the β barrel become separated in the density map. At 4.0-Å resolution, the loops connecting the strands were constructed, the main chain of the protein subunit was traced, and a polyaniline model consisting of 173 residues out of a maximum of 194 residues (the first 26 residues of the CP were digested prior to the crystallization) was built into the electron density. This model was subjected to cycles of positional refinement by using Powell minimization with the program X-PLOR. The improved model gave calculated phases that were then refined by real-space symmetry averaging with the program RAVE. The resultant electron density shows side chains at a number of positions along the main chain (Fig. 1). However, a complete assignment of the amino acid sequence to the electron density cannot be accomplished in the absence of high-resolution diffraction data. The subunit model was further improved by providing good overall hydrogen-bonding patterns and stereo-

TABLE 2. Statistics on data collection and phase refinement for AMV^a

Resolution range (Å)	No. of unique reflections	Observed data (%)	R factor	CC
50.0–8.62	5,243	86.5	0.233	0.852
8.62–6.84	5,038	84.0	0.272	0.788
6.84–5.98	4,827	80.5	0.292	0.705
5.98–5.43	4,635	77.7	0.303	0.673
5.43–5.04	4,356	72.9	0.354	0.609
5.04–4.74	4,504	75.3	0.342	0.546
4.74–4.51	4,215	70.4	0.348	0.500
4.51–4.31	3,754	62.9	0.407	0.325
4.31–4.14	3,309	55.6	0.431	0.218
4.14–4.00	2,784	47.1	0.552	0.160
50.0–4.00	42,665	71.3	0.323	0.770

^a AMV diffraction data were collected on a GX20 Elliott rotating anode X-ray generator using oscillation photography by Fita et al. (11). Film processing indexing, and postrefinement of the data were earlier reported (2) and have been repeated with improved versions of the programs to obtain a better-quality data set. Rotation function and crystal packing analyses were also repeated and were found to agree with the previously reported results (2). An initial set of phases for data between 20 and 15 Å was computed from the model built by Fita et al. (11), using the program X-PLOR (6). The phase refinement and extension were performed by 20-fold noncrystallographic real-space symmetry averaging by using the program RAVE (18) and back transforming the density to a higher resolution. Number of films processed = 253 (165 A films and 88 B films).

chemistry of the secondary structure elements. A comparison of the observed structure factors (F_{obs}) with those calculated from the model [$F_{\text{calc}}(\text{model})$] gives the crystallographic R factor and the correlation coefficient (CC) as 44.2 and 65.0%, respectively. Comparison of F_{obs} with the calculated structure factors from the averaged density [$F_{\text{calc}}(\text{density})$] gives better statistics (R factor = 32.3% and CC = 77.0% [Table 2]). A comparison of the statistics for phase refinement between the reprocessed data and those of Fukuyama et al. (12) is shown in Table 1 at the comparable resolution (4.5 Å).

The electron density map shows that the T=1 particle is roughly spherical, with a maximum diameter of ~220 Å. The shell of the particle, about 50 Å thick, is built from 60 copies of the CP standing "end on" on the viral surface; i.e., the body axis of CP is almost parallel to the closest fivefold axis such that the subunits appear to protrude out radially. The particle is characterized by the presence of prominent holes (~35 Å in diameter) at the icosahedral fivefold axes that traverse the entire thickness of the protein shell. The CP was found to have the canonical eight-stranded β -barrel fold which is common to the structures of most spherical viruses (Fig. 2). The dimensions of the β barrel are ~35 Å along the long axis and ~13 Å along the short axis. A novel feature of the AMV subunit is the EF loop of the β -barrel, which is comprised of two β strands that wrap around the barrel and run almost perpendicular to the strand direction. The N-terminal and C-terminal arms in the model are extended chains.

The interaction of the CP with its neighboring subunits is primarily limited to its two- and threefold related partners (Fig. 3). The current density map is best fit by extending the C-terminal arm of the CP toward the N-terminal arm of the twofold related subunit and hooking it around the N terminus. The C terminus of one subunit is sandwiched between the N-terminal arm and the body of the β barrel of the partner. The clamping of the C-terminal arms of the subunits is the basis of the dimer formation in the T=1 particle, a phenomenon also observed in DNA tumor papovaviruses, simian virus 40 (19), polyomavirus (29), and cowpea chlorotic mottle virus

(CCMV) (28). Although the electron density near the clamping region is not very well resolved, the constraints of the icosahedral symmetry are consistent with the dimer interaction described. The dimer is further stabilized by interactions between the C-terminal arms at the icosahedral twofold axis. At the current resolution, it is impossible to assign the density to a specific amino acid. Inspection of this electron density suggests either a stacking interaction between the side chains of symmetry-equivalent residues in the two subunits or a metal ion binding site. The latter possibility is supported by biochemical studies of Sehne et al. (26, 27) that proposed binding of one Zn atom to a dimer of AMV CP. The subunits at the trimer in the T=1 particle have extensive interactions around the threefold rotation axis. The subunits forming the pentamers have the least interaction with each other.

The present structure confirms the analysis of Fukuyama et

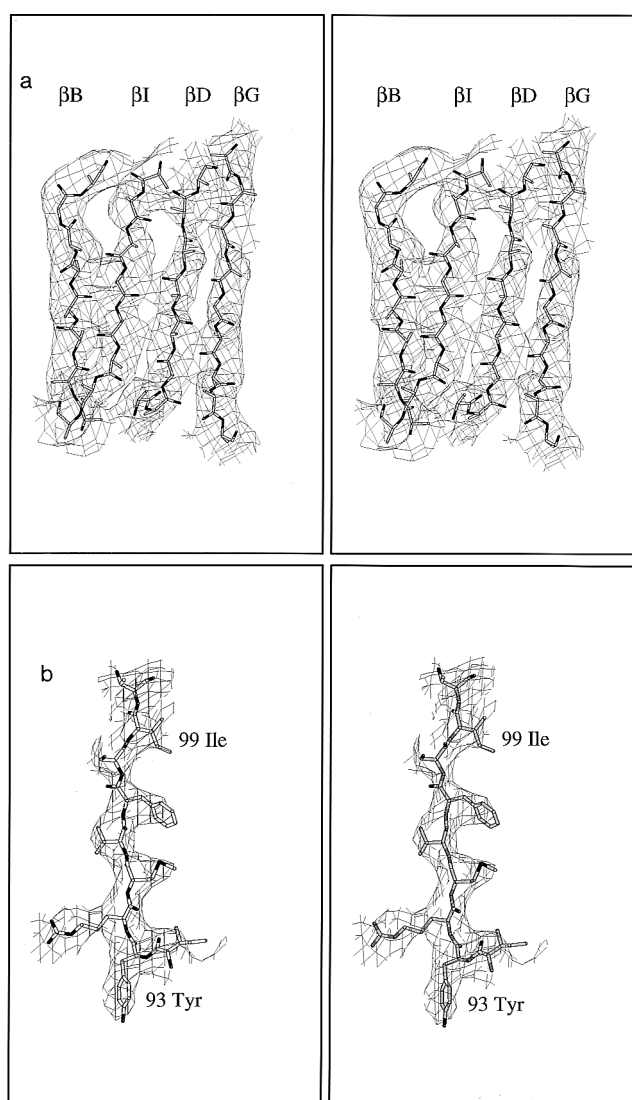


FIG. 1. Sections of the averaged electron density with the model showing the overall quality of the map at 4.0-Å resolution. The BIDG wall (comprised of strands β B, β I, β D, and β G) of the β -barrel (a) clearly shows the individual strands, with occasional side chain density budding out from the main chain. The side chain densities are more prominent at other places in the model such as shown in panel b, which probably corresponds to amino acids 92 to 100 (TYRMYFSIT).

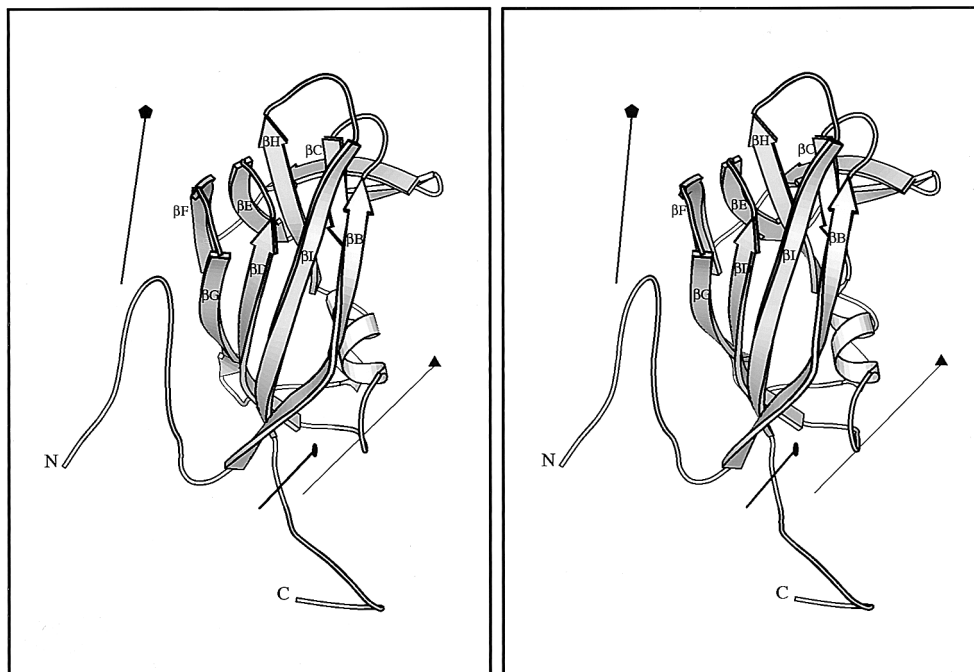


FIG. 2. A stereo view of the ribbon diagram showing the tertiary structure of AMV CP. The secondary structure elements of the β barrel are labeled according to the standard convention. The particle exterior is at the top of the diagram. Also shown are icosahedral symmetry axes (two-, three-, and fivefold rotation axes, represented by ovals, triangles, and pentagles, respectively) indicating the relative orientation of the CP with respect to these axes.

al. (12) regarding the overall description of the particle and the occurrence of holes at fivefold axes. It also shows that the CP adopts the β -barrel structure.

Our efforts to assign the amino acid sequence to the polyaniline model have not been successful despite the use of the heavy-atom data. Fukuyama et al. (12) had initially obtained a 5.0-Å structure of AMV with the single isomorphous replace-

ment method when two cysteine residues (Cys 108 and Cys 169) were labeled with Hg atoms by using *p*-hydroxymercuri-phenyl sulfonic acid. The positions of these Hg atoms and the two Cys residues were used as a guide to assign the sequence to the model without much avail. The density for the current model clearly corresponds to the correct phase enantiomorph because the helices are right handed and the twist of the strands in the β sheets is correct. It is possible, however, that in the manipulations used to determine the phases, a hand change occurred relative to the heavy-atom positions reported by Fukuyama et al. (12). To account for this possibility, we have explored all of the noncrystallographic symmetry related positions of Hg atoms as reported by Fukuyama et al. (12) as well as their enantiomorph equivalent positions. The positions of the Hg atoms relative to the assignment of residue numbers (1 is the first residue visible at the N terminus of the model) in the CP subunit are shown in Table 3. Although the heavy-atom positions cluster around the CP, assigning cysteine 108 and 169 to the nearest possible residues in the model seems inconsistent with the current interpretation of the main chain fold. In the light of the heavy-atom data, the best fit would be to assign Cys 169 to residue 119 in the model. This implies that the model in Fig. 2 starts at residue ~ 50 and ends at residue ~ 220 , with slight adjustments. Both of these termini are reasonable since 26 residues were removed from the N terminus by proteolytic treatment and the last residue in the sequence is at position 220. This, however, prevents a consistent assignment to Cys 108, as the closest Hg atom is ~ 12 Å away from the assigned residue. These inconsistencies lead to repeated critical analysis of the main chain tracing of the CP. The electron density clearly indicates that the CP adopts the canonical β -barrel fold. The β -sandwich structure of the CP is further supported by the occurrence of this canonical fold in CCMV, also a member of the *Bromoviridae* family of plant viruses. It may be pointed out that there is a slight possibility of

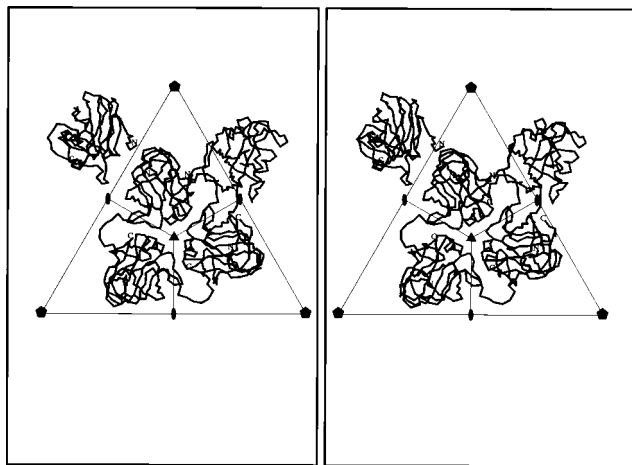


FIG. 3. A stereo view of the subunits as a C_α tracing showing the interactions among the symmetry related partners in the T=1 icosahedral AMV particle. The view shows the subunits looking down the threefold rotation axis. The icosahedral symmetry axes are labeled by symbols (ovals, triangles, and pentagles) representing the two-, three-, and fivefold rotation axes. The interaction underlying the dimer formation through the hooking of the C-terminal arm of a subunit around the N-terminal arm of the dimer can be seen between the subunits at the right side of the triangle. The trimer interactions are most prominent near the threefold icosahedral axis and along the subunit interface. The pentamer interactions are very weak.

TABLE 3. Disposition of the heavy-atom sites relative to the CP subunit^a

Hg atom	Nearest residue ^b	Distance (Å)	Effect of assigning the residue in column 2 to:	
			Cys 108	Cys 169
Hg-A	119	2.21	Negative N terminus	Best possible assignment
Hg-B	30	38.1	C terminus beyond 220	C terminus beyond 220
Hg-A3	161	3.71	Negative N terminus	N terminus at residue 9
Hg-A'	22	1.92	C terminus beyond 220	C terminus beyond 220

^a The two Hg atom coordinates corresponding to the sites reported by Fukuyama et al. (12) were used to generate two enantiomorphic equivalent sites by inverting the coordinates across the center of the virus. A set of 80 (20×4) sites was then obtained from these four sites by the application of the 20 noncrystallographic symmetry operators. These sites were screened for their proximity to the reference CP subunit, and finally four positions that fall within a cutoff distance of 4.0 Å from any of the residues in the CP were selected. Sites Hg-A and Hg-B correspond to those reported by Fukuyama et al. (12). Hg-A3 is related to the site Hg-A by a threefold noncrystallographic symmetry operation. Site Hg-A' is the enantiomorphic equivalent site to Hg-A. The residues closest to these sites, listed in column 2, are at a distance (measured from atom C_β) shown in column 3. Columns 4 and 5 describe the effects of assigning the residue in column 2 to Cys 108 and Cys 169, respectively. Thus, if residue 119 is assigned to Cys 108, then the resultant N terminus would end up at -9. It should be noted that the AMV CP has 220 residues and that the first 26 residues were cleaved prior to crystallization.

^b The model is numbered 1 to 173 from N terminus to the C terminus and does not correspond to the actual numbers of the amino acid sequence.

labeling His residues (there are seven His and three Cys residues in the sequence) with *p*-hydroxymercuriphenyl sulfonic acid, as noted by Hermodson (12). Therefore, definitive assignment of the sequence to the polyaniline model will have to await the collection of higher-resolution X-ray diffraction data when better-quality crystals are produced.

EM analysis. The electron microscopic (EM) reconstruction of the AMV T=1 particle and the X-ray model superimposed into the EM electron density show excellent agreement (Fig. 4). No discrepancy between the EM density and the X-ray structure could be detected at 27-Å resolution. The cryoEM model confirms the presence of the large holes at the pentamer axes observed in the X-ray structure.

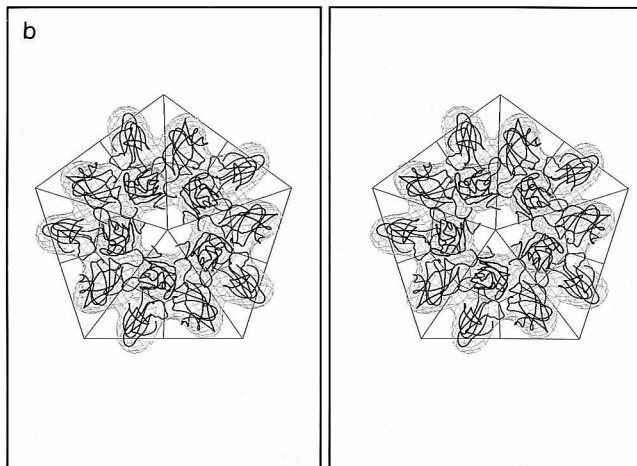
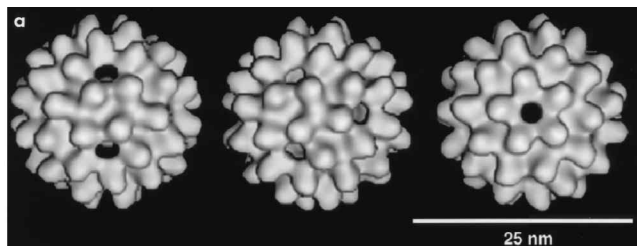


FIG. 4. A 27-Å cryoEM image reconstruction of the T=1 icosahedral AMV particle shown down the two-, three-, and fivefold symmetry axes (from left to right). (b) The stereo view of the 4.0-Å X-ray structure superimposed into the EM density down the icosahedral fivefold axis showing the presence of a wide hole (~35 Å in diameter).

The AIMV subunit structure and dimer association shows a strong structural similarity to CCMV (28). Both viruses have coat proteins, each with the β sandwich oriented end on compared with southern bean mosaic virus (1) or tomato bushy stunt virus (14). Both viruses have interlocking termini stabilizing the dimers, and both have openings at the pentamer axes. The holes are very different, however, in that CCMV is nearly sealed by side chain interactions while the AMV interior is accessible to a spherical probe with a radius of greater than 17 Å! Such a porous particle structure is consistent with the digestion of AMV RNA when virions are exposed to RNase *in vitro* (5). It seems remarkable that the tenuous protection of the genome provided by this capsid is sufficient to allow productive transport of the nucleic acid between hosts. Modeling experiments and negative-stain EM (8, 15, 20, 21) suggest that the hexamer-based cylindrical lattice of the naturally occurring bacilliform particles has openings at sixfold axes that are at least as large as those at the pentamers in the T=1 particle.

CryoEM analysis of the bacilliform particles is currently under way, and models based on the AMV subunit and quaternary structure have been developed to help characterize the protein-nucleic acid interactions in the bacilliform particles. These studies aim to better understand how such a porous particle can protect the RNA genome and to determine the advantages that such an organization affords the virus.

ACKNOWLEDGMENTS

The work on AMV was supported by NSF grant PCM78-16584 and NIH grant AI11219 to M.G.R. in the early 1980s. The recent work on AMV was supported by NIH grant GM54076 to J.E.J., USDA grant 90-34190-5207 to V.Y., and NSF grant MCB 9206305 and Program Project grant AI35212 from the Public Health Service to T.S.B.

The extensive help of Marleen Foda in purifying and crystallizing AMV in the 1980s is greatly appreciated.

REFERENCES

1. Abad-Zapatero, C., S. S. Abdel-Meguid, J. E. Johnson, A. G. W. Leslie, I. Rayment, M. G. Rossmann, D. Suck, and T. Tsukihara. 1980. Structure of southern bean mosaic virus at 2.8 Å resolution. *Nature* **286**:33-39.
2. Abdel-Meguid, S. S., K. Fukuyama, and M. G. Rossmann. 1982. The orientation of a T = 1 assembly of alfalfa mosaic virus coat protein in a hexagonal crystalline array. *Acta Crystallogr.* **B38**:2004-2008.
3. Baker, T. S., W. W. Newcomb, N. H. Olson, L. M. Cowser, C. Olson, and J. C. Brown. 1991. Structures of bovine and human papillomaviruses. Analysis by cryoelectron microscopy and three-dimensional reconstruction. *Biophys. J.* **60**:1445-1456.
4. Bol, J. F., B. Kraal, and F. T. Brederode. 1974. Limited proteolysis of alfalfa mosaic virus: influence on the structural and biological function of the coat protein. *Virology* **58**:101-110.
5. Bol, J. F., and H. Veldstra. 1969. Degradation of alfalfa mosaic virus by pancreatic ribonuclease. *Virology* **37**:74-85.

6. **Brünger, A. T.** 1993. X-PLOR version 3.1 manual. Yale University, New Haven, Conn.
7. **Collaborative Computational Project, Number 4.** 1994. The CCP4 suite: programs for protein crystallography. *Acta Crystallogr.* **D50**:760–763.
8. **Creemers, A. F., G. T. Oostergetel, M. J. Schilstra, and J. E. Mellema.** 1981. An electron microscopic investigation of the structure of alfalfa mosaic virus. *J. Mol. Biol.* **145**:545–561.
9. **Driedonks, R. A., P. C. Krijgsman, and J. E. Mellema.** 1977. Alfalfa mosaic virus protein polymerization. *J. Mol. Biol.* **113**:123–140.
10. **Driedonks, R. A., P. C. Krijgsman, and J. E. Mellema.** 1976. A study of the states of aggregation of alfalfa mosaic virus protein. *Philos. Trans. R. Soc. Lond. Ser. B* **276**:131–141.
11. **Fita, I., Y. Hata, and M. G. Rossmann.** Unpublished data.
12. **Fukuyama, K., S. S. Abdel-Meguid, J. E. Johnson, and M. G. Rossmann.** 1983. Structure of a $T=1$ aggregate of alfalfa mosaic virus coat protein seen at 4.5 Å resolution. *J. Mol. Biol.* **167**:873–894.
13. **Fukuyama, K., S. S. Abdel-Meguid, and M. G. Rossmann.** 1981. Crystallization of alfalfa mosaic virus coat protein as a $T=1$ aggregate. *J. Mol. Biol.* **150**:33–41.
14. **Harrison, S. C., A. J. Olson, C. E. Schutt, F. K. Winkler, and G. Bricogne.** 1978. Tomato bushy stunt virus at 2.9 Å resolution. *Nature* **276**:368–373.
15. **Hull, R.** 1969. Alfalfa mosaic virus. *Adv. Virus Res.* **15**:365–433.
16. **Hull, R., G. J. Hills, and R. Markham.** 1969. Studies on alfalfa mosaic virus. II. The structure of the virus components. *Virology* **37**:416–28.
17. **Jones, T. A., S. Cowan, J. Y. Zou, and M. Kjeldgaard.** 1991. Improved methods for building protein models in electron density maps and the location of errors in these models. *Acta Crystallogr. A* **47**:110–119.
18. **Kleywegt, G. J., and T. A. Jones.** 1994. Halloween—masks and bones, p. 59–66. *In* S. Bailey, R. Hubbard, and D. Waller (ed.), *From first map to final model*. SERC Daresbury Laboratory, Warrington, England.
19. **Liddington, R. C., Y. Yan, J. Mouli, R. Sahli, T. L. Benjamin, and S. C. Harrison.** 1991. Structure of simian virus 40 at 3.8Å resolution. *Nature* **354**:278–284.
20. **Mellema, J. E.** 1975. Model for the capsid structure of alfalfa mosaic virus. *J. Mol. Biol.* **94**:643–648.
21. **Mellema, J. E., and H. J. van den Berg.** 1974. The quaternary structure of alfalfa mosaic virus. *J. Supramol. Struct.* **2**:17–31.
22. **Murphy, F. A., C. M. Fauquet, D. H. L. Bishop, S. A. Ghabrial, A. W. Jarvis, G. P. Martelli, M. A. Mayo, and M. D. Summers (ed.).** 1995. *Virus taxonomy*. Springer-Verlag, Vienna, Austria.
23. **Olson, N. H., T. S. Baker, J. E. Johnson, and D. A. Hendry.** 1990. The three-dimensional structure of frozen-hydrated *Nudaurelia capensis* beta virus, a $T = 4$ insect virus. *J. Struct. Biol.* **105**:111–122.
24. **Rossmann, M. G.** 1979. Processing oscillation diffraction data for very large unit cells with an automatic convolution technique and profile fitting. *J. Appl. Crystallogr.* **12**:225–238.
25. **Rossmann, M. G., A. G. W. Leslie, S. S. Abdel-Meguid, and T. Tsukihara.** 1979. Processing and post-refinement of oscillation camera data. *J. Appl. Crystallogr.* **12**:570–581.
26. **Senhke, P. C., and J. E. Johnson.** 1994. A chromatographic analysis of capsid protein isolated from alfalfa mosaic virus: zinc binding and proteolysis cause distinct charge heterogeneity. *Virology* **204**:843–846.
27. **Sehnke, P. C., A. M. Mason, S. J. Hood, R. M. Lister, and J. E. Johnson.** 1989. A “zinc finger”-type binding domain in tobacco streak virus coat protein. *Virology* **168**:48–56.
28. **Speir, J. A., S. Munshi, G. Wang, T. S. Baker, and J. E. Johnson.** 1995. Structures of the native and swollen forms of cowpea chlorotic mottle virus determined by X-ray crystallography and cryo-electron microscopy. *Structure* **3**:63–78.
29. **Stehle, T., Y. Yan, T. L. Benjamin, and S. C. Harrison.** 1994. Structure of murine polyomavirus complexed with an oligosaccharide receptor fragment. *Nature* **369**:160–163.
30. **Tong, L. A., and M. G. Rossmann.** 1990. The locked rotation function. *Acta Crystallogr. Sect. A* **46**:783–792.
31. **Van Vloten-Doting, L., and E. M. Jaspars.** 1972. The uncoating of alfalfa mosaic virus by its own RNA. *Virology* **48**:699–708.
32. **Winkelmann, D. A., T. S. Baker, and I. Rayment.** 1991. Three-dimensional structure of myosin subfragment-1 from electron microscopy of sectioned crystals. *J. Cell Biol.* **114**:701–713.
33. **Yusibov, V., A. Kumar, A. North, J. E. Johnson, and L. S. Loesch-Fries.** 1996. Purification, characterization, assembly and crystallization of assembled alfalfa mosaic virus coat protein expressed in *Escherichia coli*. *J. Gen. Virol.* **77**:567–573.